Dual-Plating Aqueous Zn-Iodine batteries Enabled by Halogen-Complexation Chemistry for Large-Scale Energy Storage

Hong Li[1,3#], Bosi Huang[1#], Mingyan Chuai[4,5#], Zhiyang Zheng[1], Hao Chen[2], Zhihong Piao[1], Guangmin Zhou[1]*, Hong Jin Fan[2,3]*

[1]Tsinghua Shenzhen International Graduate School, Tsinghua University, Shenzhen, 518055, China

[2]School of Physical and Mathematical Sciences, Nanyang Technological University, Singapore 637371

[3]Energy Research Institute @ NTU (ERI@N), Nanyang Technological University, Singapore 637553

[4]State Key Laboratory of Structural Chemistry, Fujian Institute of Research on the Structure of Matter, Chinese Academy of Sciences, Fuzhou 350002, Fujian, China.

[5]Mindu Innovation Laboratory, Fujian Science & Technology Innovation Laboratory for Optoelectronic Information of China, Fuzhou 350108, Fujian, China.

Corresponding authors: guangminzhou@sz.tsinghua.edu.cn; fanhj@ntu.edu.sg

Methods

Chemicals and Materials

Zinc iodide (ZnI_2, ⩾ 98%), tetraglyme (G4, 99%) were purchased from Macklin. Potassium iodide (KI, 99%), zinc sulfate heptahydrate ($ZnSO_4 \cdot 7H_2O$, 99.5%) were purchased from Aladdin company. Graphite felt and Zn anode were purchased from Tan Qianlang new materials company and Shengshida Metal Materials Company, respectively. Deionized water was used for preparing the electrolytes.

Battery Assembly and Test

For the static cell, the electrolytes were prepared after all the components (6 g

$ZnSO_4 \cdot 7H_2O$, 4 g ZnI_2, 2 g KI, and 27 mL H_2O) were stirred for thorough mix. Then, 2.7 g G4 was dropped into the stirring solution. A graphite felt (1.5 cm × 1 cm × 0.6 cm) electrode was immersed into the prepared 20 mL electrolytes to serve as the cathode. A zinc plate (1.5 cm × 1.5 cm × 0.08 cm) located at the bottom of the cylindrical cell served as the anode. For the flow batteries, the I^- concentration of the electrolytes was increased to 4 M.

The rate performance and long-cycling performance were charged/discharged with a constant current. The rate performance of the applied current was in the range of (5~25 mA cm^{-2}). All the measurements were carried out at room temperature under an ambient atmosphere.

Characterizations

X-ray photoelectron spectroscopy (XPS) was characterized using an AXIS Ultra DLD-type X-ray photoelectron spectrometer (Shimadzu, Japan) equipped with the monochromatic Kα radiation of the Al target as the X-ray source (1486.6 eV) and the binding energy of the C 1s peak (284.6 eV). X-ray diffraction (XRD) patterns were recorded on a D8 DaVinci X-ray diffractometer (Bruker, Germany) with a test angle range of 5-80° (2θ) and a rate of 10°/min. Raman spectroscopy was conducted on an In Via Qontor confocal micro-Raman spectrometer (Renishaw, UK) to characterize the solvation structure of the electrolyte. Raman measurements were acquired using a Horiba LabRAM HR Evolution at 532 nm. A confocal laser scanning microscope (CLSM, VK−X1000, KEYENCE) was used to analyze the roughness of the surface after cycling at a large area. Fourier transform infrared (FTIR) spectra were recorded on a Nicolet 6700 infrared spectrometer from Thermo Fisher Scientific (USA).

In situ optical microscopy detection was carried out by using a homemade electrochemical device. Graphite felt electrode with the size of 2 cm*2 cm*0.4 mm and a piece of Zn anode with the thickness of 0.5 mm were used as the positive and negative electrode, respectively. The battery was charged via an electrochemical workstation (LANHE, Wuhan) at a current of 1 mA. An optical microscope (Leica microsystems CMS GmbH) was used to detect the I_2 plating on the surface of graphite felt.

In-situ ultraviolet detection was carried out by using a homemade electrochemical device. Spectroelectrochemical experiments were performed in a quartz UV-visible cell. The positive and negative electrodes were a piece of graphite felt and zinc metal, respectively. The total volume of electrolytes was 3.35 mL. The battery was charged/discharged via an electrochemical workstation (LANHE, Wuhan) at a current of 0.2 mA. UV-visible absorption spectra were background-subtracted for the pristine electrolyte contribution (recorded as a blank and automatically subtracted from subsequent spectra) prior to the electrochemical or chemical reactions.

Density functional theory (DFT) calculations

Density functional theory (DFT) calculations were conducted using the CP2K/Quickstep software suite. The Perdew-Burke-Ernzerhof (PBE) functional was utilized to determine the electronic structure, with van der Waals interactions included via the Grimme D3 dispersion correction. A plane-wave cutoff of 500 Ry was employed to ensure the accurate expansion of the wavefunction, complemented by a Triple-Zeta Valence with Polarization (TZVP) basis set. For high precision in electronic calculations, the self-consistent field (SCF) criterion was set to a strict convergence threshold of 1×10^{-6} Hartree. Static geometry optimizations were performed using the Broyden-Fletcher-Goldfarb-Shanno (BFGS) algorithm to ensure reliable structural convergence. Solvation effects were simulated using the Polarizable Continuum Model (PCM), where the solvent environment was represented as a dielectric continuum with a dielectric constant of 45.0.

MD simulations

MD simulations for the electrolyte structures were conducted by using the GROMACS package. GAFF force field [1] was used to model G4 molecule. Parameters of Zn^{2+}, K^{+}, and I^{-} were obtained from the work of Merz et al. [2]. Water molecule was modelled by SPC/E model[3]. The Z, ZI(1.2 M)G, and ZI(1.2 M)G electrolyte structures were simulated by the same concetration of the I^{-}. The radial distribution functions (RDFs) were calculated by the in-built module. The snapshot of MD simulation was produced by VMD software.

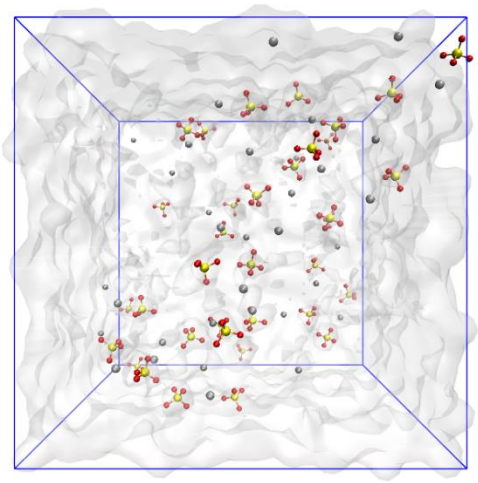

Fig. S1 The MD snapshots of Z electrolytes.

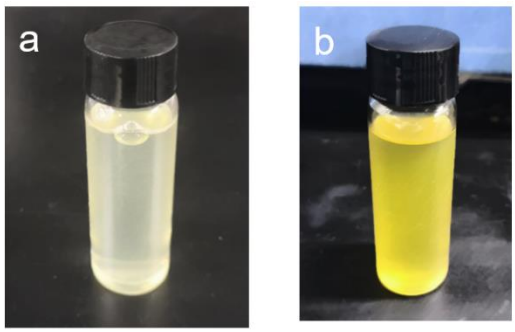

Fig. S2 Digital photos of the ZI (a) and ZIG (b) electrolytes.

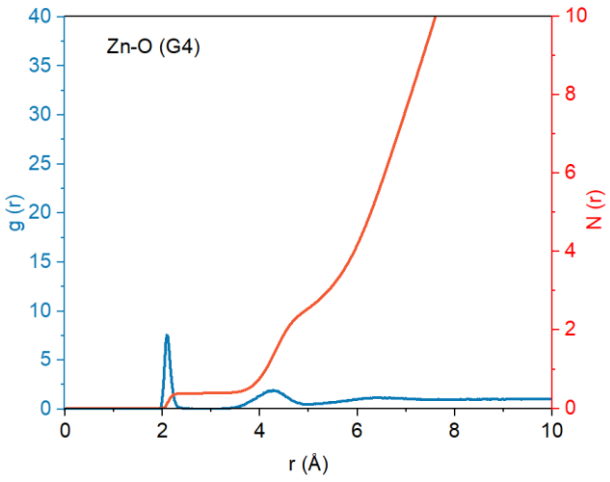

Fig. S3 Radial distribution functions and the coordination number for Zn-O (G4) in ZIG electrolytes.

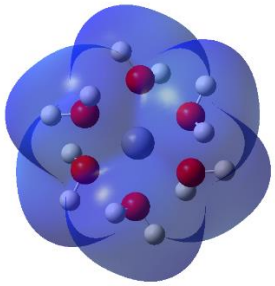

Fig. S4 Electrostatic potential distributions of $Zn(H_2O)_6^{2+}$.

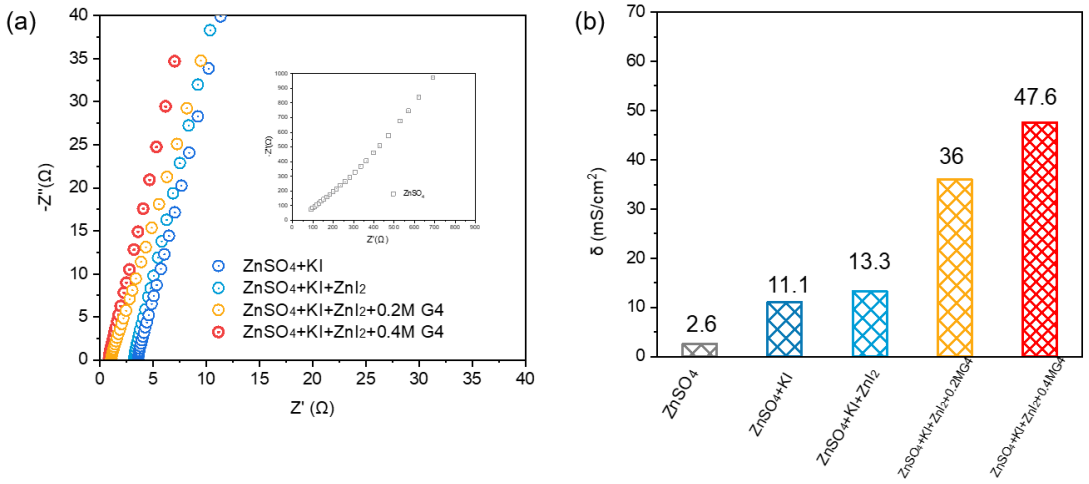

Fig. S5. (a) Nyquist plots collected at open circuit voltage (OCV) over the frequency range of 100 kHz to 0.1 Hz in different electrolytes. (b) Ionic conductivity comparison of different electrolytes.

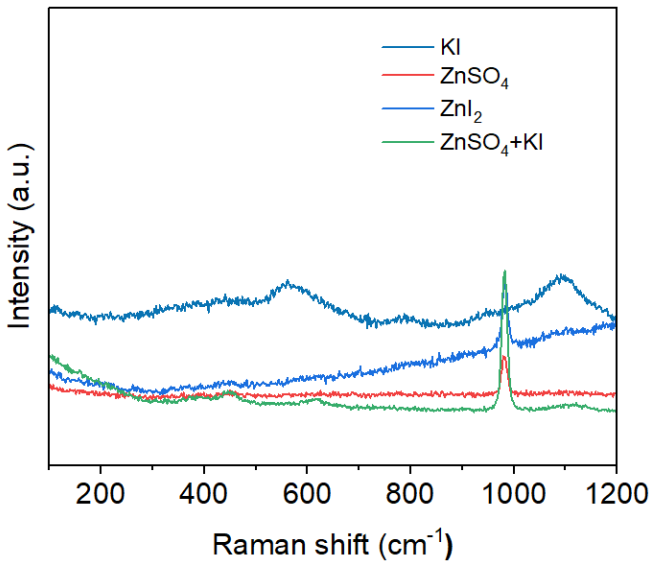

Fig. S6 Raman spectra of KI, $ZnSO_4$, ZnI_2, $ZnSO_4$+KI electrolytes.

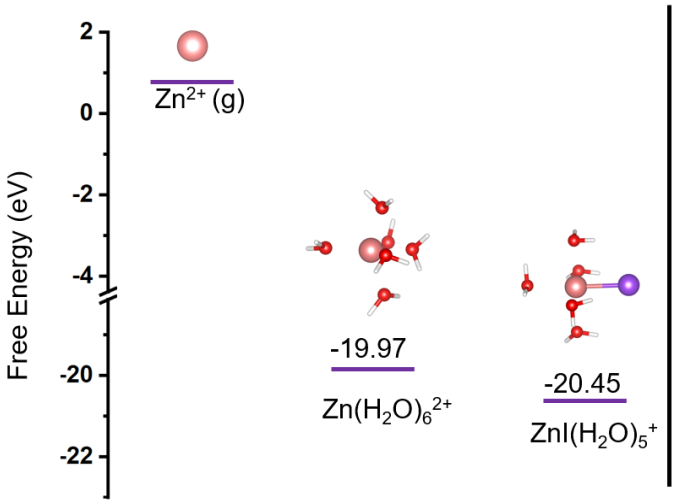

Fig. S7 Free energy change in the Zn^{2+} solvation in the ZI electrolytes.

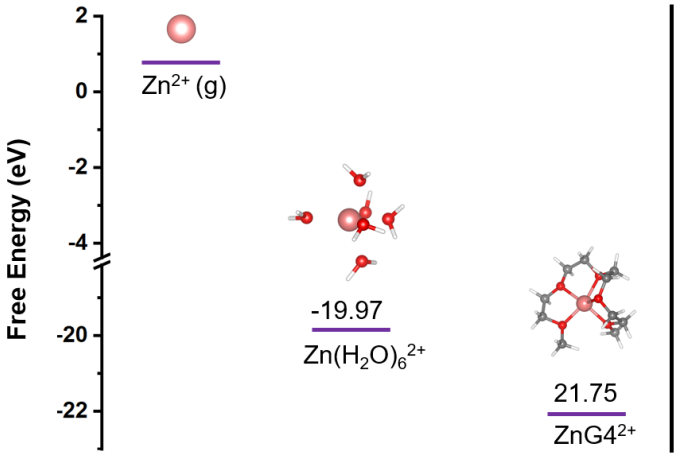

Fig. S8 Free energy change in the Zn^{2+} solvation in the $ZnSO_4$/G4 electrolytes.

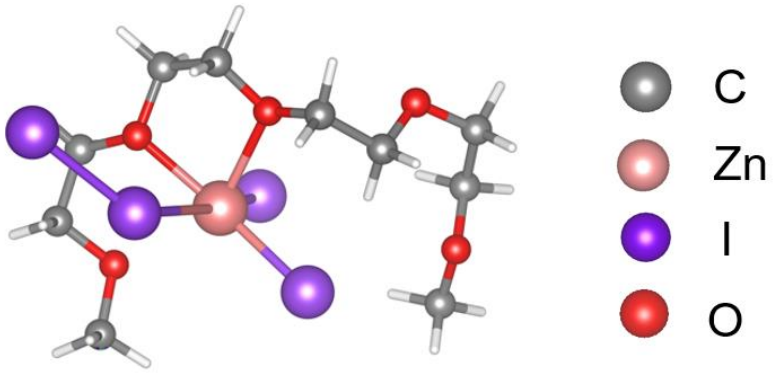

Fig. S9 The structure of ZnI_4G4^{2-} from DFT calculations. The calculated ZnI_4G4^{2-} is unstable as the extra iodine cannot bind with Zn^{2+}.

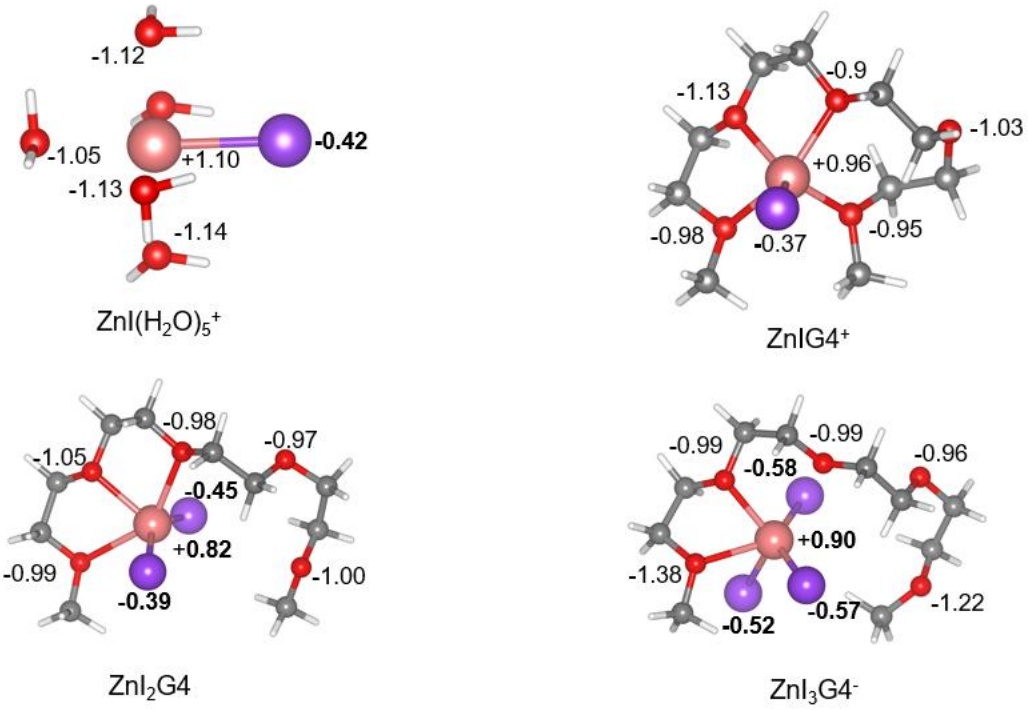

Fig. S10 The solvation structure and atomic charge of $ZnI(H_2O)_5^+$, $ZnIG4^+$, ZnI_2G4, and ZnI_3G4^-.

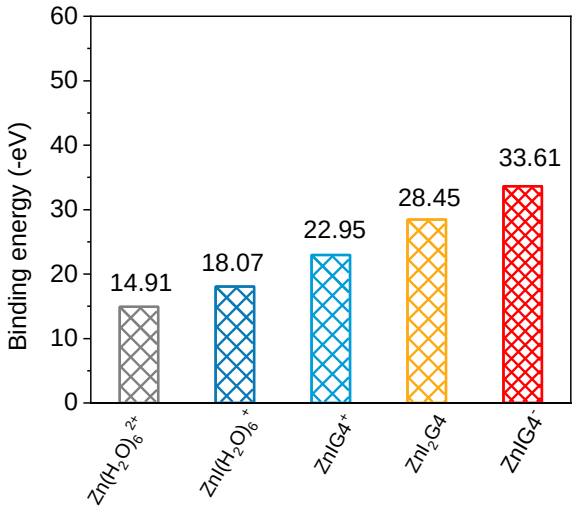

Fig. S11 The binding energy of the various solvation structures.

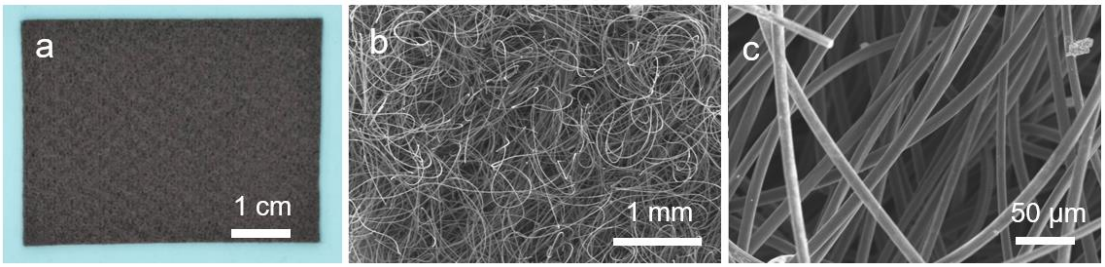

Fig. S12 Digital photo (a) and SEM images (b,c) of the graphite felt.

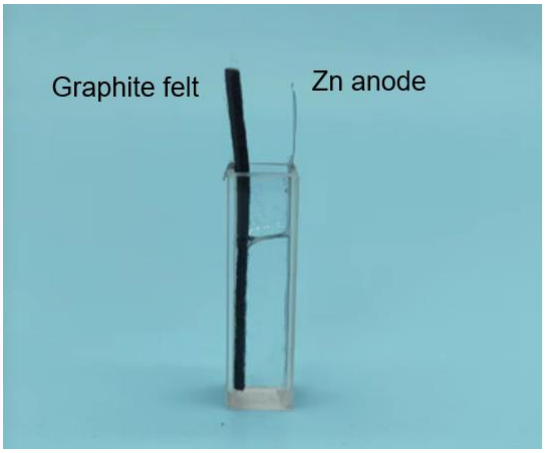

Fig. S13 The configuration of *in-situ* UV-vis for detecting polyiodides species.

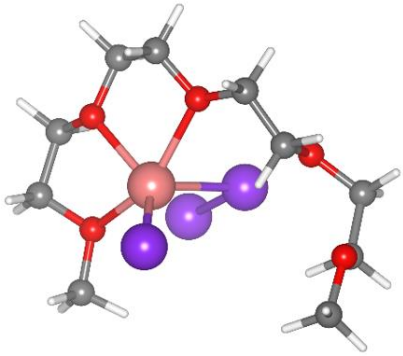

Fig. S14 The structure of ZnI_3G4^+ from DFT calculations. The obtained E_b is -15.2 eV.

Note: The Raman peak of the polyiodide in the ZIG electrolytes locates at 114 cm^{-1} after charging (Figure 4f). This position is higher than that of free I_3^- at 104 cm^{-1} (Fig. S17b). Such an buleshift indicates that the binding interaction of G4 with polyiodines in the ZIG electrolytes, diminishing the free polyiodines species[5].

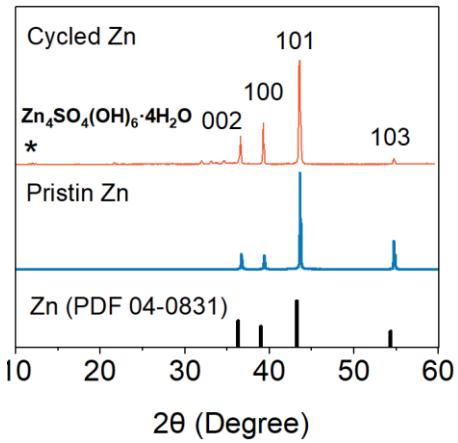

Fig. S15 XRD patterns of the zinc anode before and after cycling.

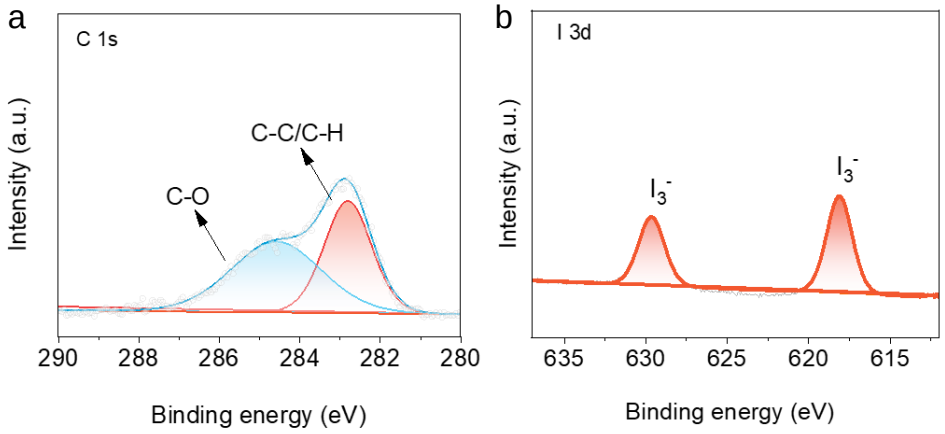

Fig. S16 XPS spectra of the cycled zinc anode (a) C 1s, (b) I 3d.

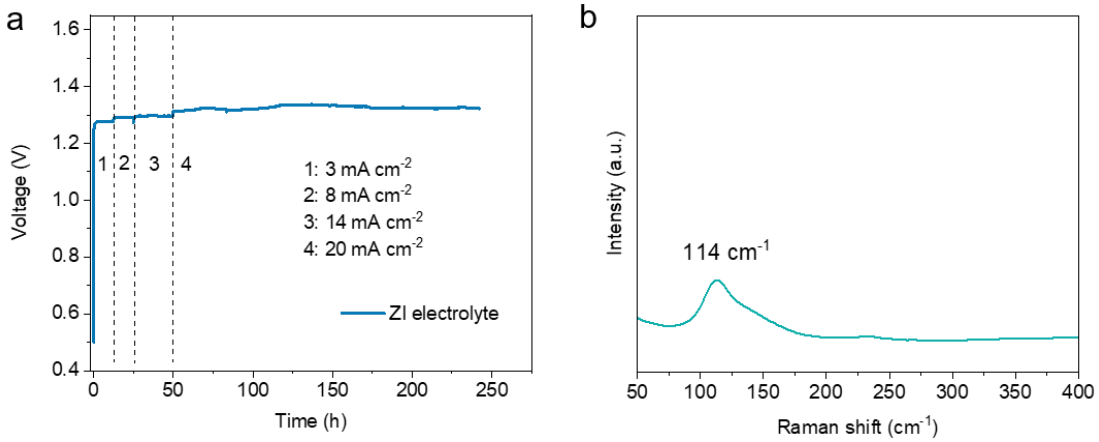

Fig.S 17 (a) Time-voltage curve of the battery with the ZI electrolytes at different charging currents; (b) Raman spectra of the ZI electrolytes after charging.

During charging, the voltage first increases and then decreases at increasing currents. However, it never reaches the cutoff charging voltage of 1.4 V (versus Zn/Zn^{2+}). This is because, during charging, free I_3^- are produced and no I_2 molecules are plated on the graphite felt. As a result, no capacity is observed during discharging.

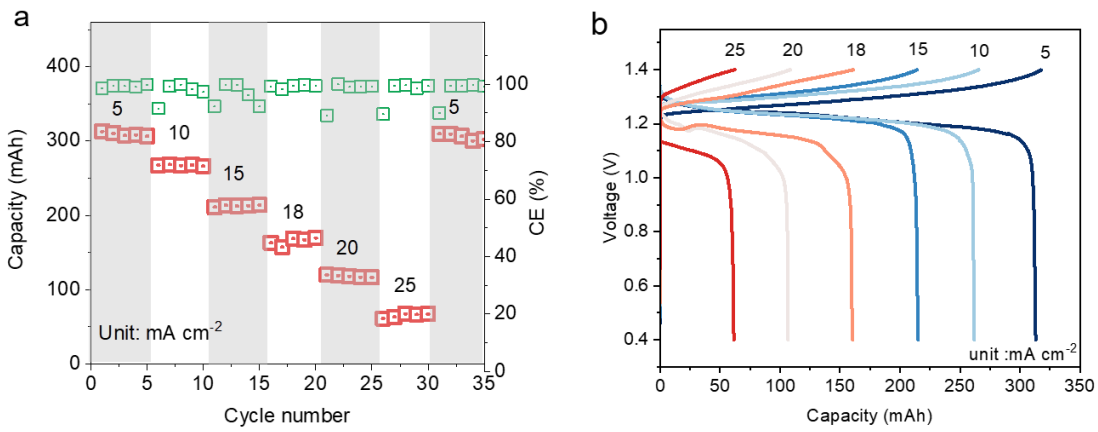

Fig. S18 (a) Rate performance of DPZIB. (b) The corresponding GCD curves of the batteries at different current densities.

Fig. S19 Photographs of the assembled DPZIB for Ah-level cell tests. Upper row: the carbon film and Zn plates of different sizes used in the corresponding cells in the bottom row.

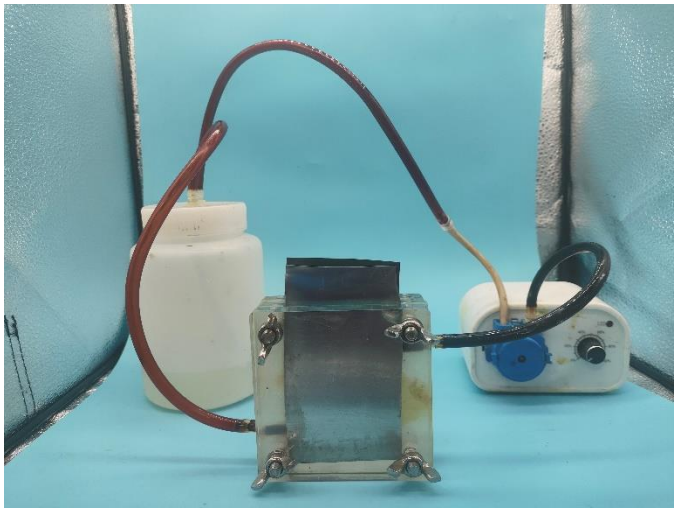

Fig. S20 Photograph of the membrane-free flow battery.

Reference

(1) Wang, J., Wolf, R. M., Caldwell, J. W., Kollman, P. A., & Case, D. A. (2004). Development and testing of a general amber force field. *J. computat. Chem.*, *25*(9), 1157-1174.

(2) Li, P.; Merz, K. M., Jr. Taking into Account the Ion-induced Dipole Interaction in the Nonbonded Model of Ions. *J. Chem. Theory Comput.* **2014**, *10* (1), 289-297.

Li, P.; Song, L. F.; Merz, K. M., Jr. Systematic Parameterization of Monovalent Ions Employing the Nonbonded Model. *J. Chem. Theory Comput.* **2015**, *11* (4), 1645-1657.

(4) Wang, J.; Wolf, R. M.; Caldwell, J. W.; Kollman, P. A.; Case, D. A. Development and testing of a general amber force field. *J. Comput. Chem.* **2004**, *25* (9), 1157-1174.

(5) Choi, G., Sullivan, P., Lv, X. L., Li, W., Lee, K., Kong, H., ... & Feng, D. Soft–hard zwitterionic additives for aqueous halide flow batteries. *Nature*, **2024**, 1-7.